Analysis of Atmospheric Delays and Asymmetric Positioning Errors in the Global Positioning System

by

Kathryn Materna

Submitted to the Department of Earth, Atmospheric, and Planetary Science
in partial fulfillment of the requirements for the degree of

Bachelor of Science in Earth, Atmospheric, and Planetary Science

at the

MASSACHUSETTS INSTITUTE OF TECHNOLOGY

June 2014

Signature redacted

Author ....
Department of Earth, Atmospheric, and Planetary Science
May 16, 2014

Signature redacted

Certified by... .....
Thomas A. Herring
Professor
Thesis Supervisor

Signature redacted

Accepted by.. .....
Richard P. Binzel
Chairman, Committee on Undergraduate Program

Analysis of Atmospheric Delays and Asymmetric Positioning Errors in the Global Positioning System

by

Kathryn Materna

Submitted to the Department of Earth, Atmospheric, and Planetary Science
on May 16, 2014, in partial fulfillment of the
requirements for the degree of
Bachelor of Science in Earth, Atmospheric, and Planetary Science

Abstract

Errors in modeling atmospheric delays are one of the limiting factors in the accuracy of GPS position determination. In regions with uneven topography, atmospheric delay phenomena can be especially complicated. Current delay models used in analyzing GPS data from the Plate Boundary Observatory (PBO) are successful in achieving millimeter-level accuracy at most locations; however, at a subset of stations, the time series for position estimates contain an unusually large number of outliers. In many cases these outliers are oriented in the same direction. The stations which exhibit asymmetric outliers occur in various places across the PBO network, but they are especially numerous in California's Mammoth Lakes region, which served as a case study for this project. The phenomenon of skewed residuals was analyzed by removing secular trends and variations with periods longer than 75 days from the signal using a median filter. The skewness of the station position residuals was subsequently calculated in the north, east and up directions. In the cases examined, typical position outliers are 5-15 mm. In extreme cases, skewed position residuals, not related to snow on antennas, can be as large as 20 mm. I examined the causes of the skewness through site-by-site comparisons with topographic data and various forms of weather data such as numerical weather models, radiosondes, and satellite images. Analysis suggests that the direction of the skewness is generally parallel to the local topographic gradient at a scale of several kilometers. Comparison with weather data suggests that outlier data points in the Mammoth Lakes region occur when lee waves are likely to form downstream of the Sierra Nevada Mountains. The results imply that coupling between the atmosphere and local topography, e.g. lee waves, is responsible for the phenomenon of skewed residuals.

Thesis Supervisor: Thomas A. Herring
Title: Professor

Acknowledgments

I am extremeley grateful to Professor Tom Herring for his guidance in forming this project and for his expertise. I am grateful for the technical help and insightful suggestions he provided. I would also like to thank the rest of Professor Herring's group, especially Mike Floyd for his help at the start of the project. I am grateful to Professor Dan Cziczo for making himself available on multiple occasions to answer my questions about atmospheric science and suggest possible directions.

I'd also like to thank my family and friends for their support. I especially appreciate my father's support and enthusiasm during this project.

Contents

List of Figures

List of Tables

Chapter 1

Introduction

Over the past several decades, the Global Positioning System (GPS) has become the most common method among scientists for measuring position around the globe. Currently, daily-averaged GPS measurements can achieve accuracies at the millimeter level, and even at the sub-millimeter level in optimal cases. The high sensitivity of GPS allows for the detection of small-amplitude phenomena such as tectonic deformation, solid earth tides, and post-seismic offsets after earthquakes. Consequently, GPS has become an important tool for many types of geophysical research.

Many of the GPS stations in the United States are part of the Plate Boundary Observatory (PBO) network. The Plate Boundary Observatory manages about 1,100 continuously-operating GPS stations throughout the United States for geophysical monitoring and research. Each station produces position estimates in the North, East, and Up directions each day, with typical position errors at these stations between 1 and 10 millimeters. For scientists who use the data to study the tectonics of North America, it is important for these measurements to be as accurate as possible.

It is observed that several GPS stations in the Sierra Nevada Mountains of California show a frequent occurrence of large position errors. Furthermore, the distribution of position outliers at these stations is strongly asymmetric about the average positions of the stations. At these stations, it appears that position errors have a preferred direction (Figure 1-1). When the time series data from these stations are de-trended, the asymmetric patterns of errors give the outliers the appearance of "dripping" from

the average station positions.

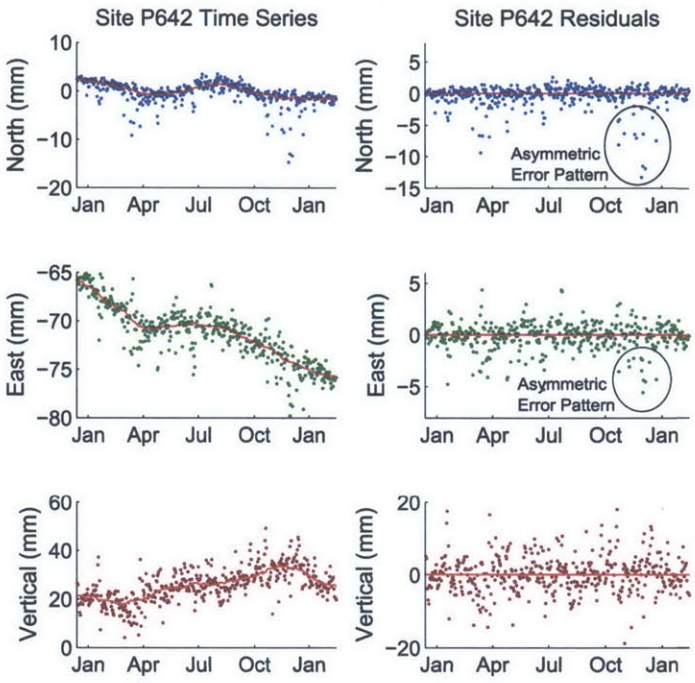

Figure 1-1: GPS time series for Site P642, a station in the Mammoth Lakes region of the Sierra Nevadas. The second set of graphs shows the same time series with the long-term trend removed so that the position errors are more apparent. Note the numerous position errors of -5 to -10 millimeters in the North and East directions, in contrast to the relatively few errors in the positive portion of each graph.

If all sources of error in each GPS measurement were correctly accounted for, then the remaining errors would be due only to random noise. In that case, the expected pattern of errors would be a symmetric normal distribution about the mean position. At the subset of stations in question, however, outliers in one direction are much more likely than outliers in the other direction. In the observed cases, the outliers have magnitudes of 5-15 millimeters. They occur 10-20 times per year, and they do not appear to be snow-related.

The presence of the asymmetric outliers indicates that a non-random source of error is affecting these GPS stations. This project addresses the question of why these specific GPS stations show an unusually large number of outliers oriented in the same

direction.

This project has particular application for GPS studies that are conducted in campaigns. In many places where scientists wish to collect geodetic data, it is impractical or prohibitively expensive to install continuous GPS devices. Instead, a campaign of GPS measurements is performed. In a campaign, a single GPS antenna is installed in a cement mount and is left to collect data for one to two days. The antenna is then moved to a different mount where it collects data for another one to two days. Several years later, the campaign is repeated. The campaign data reveal any ground motions that have occurred between the first and second measurements.

When GPS measurements are taken in a campaign format, the time spent collecting GPS data at each station is extremely limited. If the measurements were taken in a continuous fashion, the effects of random stochastic errors such as atmospheric fluctuations could be minimized by averaging over long observation periods. However, with a short set of campaign data, this type of averaging is not possible. In order to calculate accurate positions using campaign measurements, it is especially important to remove all sources of error in the data processing.

The goal of this project is to help scientists derive the most accurate position measurements possible by understanding the complex patterns of GPS position error and atmospheric delay in places like the Sierra Nevada. This knowledge will be especially applicable to the analysis of datasets from GPS campaigns in the Sierra Nevada and similar regions.

1.1 Background

1.1.1 GPS Data Processing

In order to achieve high-accuracy GPS position measurements, a number of precise correction calculations must be applied during the data analysis. These corrections account for timing errors, or errors in a receiver's ability to determine the time at which a GPS signal was emitted from a satellite. Because small errors in timing can

result in large errors in positioning, proper correction calculations must be made for as many sources of error as possible. For example, adjustments must be applied to correct for relativistic effects, fluctuations in the Earth's ionosphere, and atmospheric pressure changes at the surface of the Earth.

One of the most significant sources of error, and the most relevant for this project, is atmospheric delay. The term "atmospheric delay" accounts for the index of refraction of the atmosphere ($n_{air} \approx 1.0003$) being slightly greater than the index of refraction of a vacuum ($n_{vacuum} = 1$). As a result, GPS signals are marginally slowed and bent as they pass through the Earth's atmosphere. Atmospheric delay is measured in seconds, but is typically multiplied by the speed of light, c, so that it can be expressed in meters:

$$\Delta x = c\Delta t. \tag{1.1}$$

The value Δx is the change in distance generated by a certain amount of delay Δt in the signal propagation.

The total atmospheric delay can be separated into the component due to the "dry" gases in the atmosphere and the component due to water vapor. The delay due to each of these components is dependent on the frequency of the signal being transmitted. For systems which transmit in the microwave band of the spectrum, such as GPS and a related system called Very Long Baseline Interferometry (VLBI), the delays due to both the "dry" and the "wet" components can be calculated as functions of pressure, relative humidity, and temperature (Smith and Weintraub 1953).

If the values of pressure, relative humidity, and temperature were known to high accuracy everywhere throughout the atmosphere, then the values of atmospheric delay for GPS signals could be precisely computed by integrating the atmospheric delays along the path of each signal. This technique is called ray-tracing. However, because the values of temperature and pressure are imprecisely known in the atmosphere, current GPS analysis techniques must estimate the dry and wet atmospheric delay components. Like the estimates of station position, estimates of dry and wet atmospheric delays are included as parameters which are solved for in the GPS analysis.

The estimation of delays related to water vapor requires special consideration. The concentration of water vapor in the troposphere, related to fluctuations in the weather, is highly variable in space and time. Furthermore, unlike many other constituents of the atmosphere, water vapor has an index of refraction that depends strongly on temperature (Chao 1973). These factors combine to make delays due to water vapor particularly difficult to estimate. Errors in the water vapor component of the atmospheric delay are still one of the largest sources of positioning error in GPS analysis.

Many previous studies have examined the effects of atmospheric water vapor on positioning. Tralli et al. (1988) performed an early GPS study in the Gulf of California and showed that delay due to water vapor can be as large as 20 centimeters. This study also found that the delay related to water vapor only makes up about 10% of the total atmospheric delay, but it is typically the most difficult component to model correctly.

In GPS analysis techniques before the 2000's, atmospheric delay estimates were derived from a model of an atmosphere that was azimuthally symmetric. However, changes in technology and analysis methods improved the accuracy of GPS to such an extent that the small effects of azimuthal asymmetry could no longer be ignored. A gradient technique was then proposed to capture asymmetries by treating the atmosphere as if it were slightly tilted instead of flat. Chen and Herring (1997) used VLBI experiments to show that horizontal gradients in the atmosphere could be successfully estimated and verified using weather analysis. They showed that the degree of tilt in the East/West direction and the degree of tilt in the North/South direction could be estimated during the data processing in order to improve the accuracy of position measurements. Gradients have since become standard parameters that are estimated routinely for almost every GPS station.

Azimuthal asymmetry in the atmosphere is still a source of error in GPS processing, especially because the characteristics of the asymmetries vary from place to place. For example, Hauser (1989) showed that the presence of mountains can create an asymmetric distribution of atmospheric delay due to lee waves. Hauser, studying

laser ranging rather than GPS, showed that the Davis Mountains in Texas create asymmetric delays of up to one centimeter due to lee wave oscillations excited by the mountains. Location-specific delays of this type have not been parameterized in standard GPS processing techniques.

For this project, one area in which patterns of atmospheric delay are especially interesting is the Sierra Nevada Mountains of the Western United States. The Sierra Nevada, a 650-km long chain of mountains in California, contains some of the highest points in the continental United States. Due to the topography, atmospheric flow patterns in this area are known to be complex. The patterns of atmospheric delay over the Sierra Nevada are also complicated by the fact that the weather systems moving across the Sierra Nevada sometimes contain large amounts of water vapor absorbed over the surface of the Pacific Ocean. As a result, modeling both the "wet" and the "dry" components of atmospheric delay may present difficulties in this region.

1.1.2 Atmospheric Lee Waves

In the atmosphere, flow over uneven topography can create oscillations called lee waves downstream of topographic features. Lee waves have been studied extensively over the past century because of the interesting meteorological phenomena associated with them and because of the hazards they pose to aviation. They are especially relevant to this project for their potential effects on atmospheric delay patterns.

A very useful quantity in studying lee waves is called potential temperature. For a compressible fluid such as air, the potential temperature represents the effective temperature of a parcel of air. It is the temperature that a parcel of air would have if it were adiabatically brought to a reference pressure P_0, usually defined to be the pressure at the surface of the Earth. The potential temperature θ is defined as

$$\theta = T\left(\frac{P_0}{P}\right)^{\frac{R}{c_p}} \tag{1.2}$$

where R is the specific gas constant for air and c_p is the constant-pressure heat capacity of air. Potential temperature can be used to characterize a form of stability

in the atmosphere. In order for a column of incompressible fluid such as water to be stable and non-convecting, the temperature of the column must increase with height. Similarly, in order for the atmosphere to be stable and non-convecting, the potential temperature must increase with height. Under typical atmospheric conditions, the potential temperature increases with height.

In order for lee waves to form, the atmosphere must be stably stratified, i.e., the potential temperature of the atmosphere must increase with elevation. When the potential temperature increases upward, the lower-density fluid above a parcel of air provides a downward restoring force if the parcel is displaced upward, and the higher-density fluid below provides an upward restoring force if the parcel is displaced downward. When a parcel is displaced by a mountain or obstruction, these forces result in oscillation of the parcel in the vertical direction as the parcel travels generally downstream. Many cycles of this oscillation may occur before the energy of the perturbation is damped out.

As a displaced parcel rises and cools near the crest of each oscillation, the relative humidity of the parcel increases. The relative humidity may increase to the point where a cloud forms. As the displaced fluid leaves the crest and enters the trough of each oscillation, the relative humidity decreases again and the cloud may vaporize. This type of cloud may form at the crest of every wave, causing rows of parallel clouds to appear downwind of the obstruction. These so-called "cloud streets" are the clearest way to observe lee waves from a distance, including from satellite imagery.

The frequency of lee wave oscillations, as well as the wavelength of the resulting waves, is governed by the buoyant forces in the column of air. This frequency is called the Brunt-Väisälä Frequency, N, and is given by

$$N^2 = \frac{g}{\theta}\frac{d\theta}{dz} \tag{1.3}$$

where θ is potential temperature and g is the acceleration of gravity. When N^2 is positive, buoyant forces provide a restoring force to any perturbation, and oscillations will occur. In the case that N^2 is negative, the column is unstable and any perturba-

tion will grow exponentially. For lee waves to occur, N^2 must be positive (Glickman 2000).

Lee waves are classified into two types by the direction of the wave's momentum flux: they can be either "vertically-propagating" or "trapped" lee waves. The type and behavior of the wave is controlled by the dimensions of the topography and the vertical profiles of temperature and wind velocity in the atmosphere.

Vertically-propagating lee waves are standing internal gravity waves in which momentum is transferred upward. The energy in such a wave may propagate high into the stratosphere; vertically-propagating lee waves have been observed as high as 20 kilometers in the Sierra Nevada (Smith et al. 2008). Another characteristic property of these waves is that the first crest of the oscillations propagates upstream of the mountain range at an angle determined by wind velocity and N (Durran 2003).

Trapped lee waves, on the other hand, are waves which have horizontally-propagating momentum trapped below a capping layer of the atmosphere. These waves may exist if the atmosphere has two distinct layers, each with different properties, and the waves are unable to propagate into the upper layer. Often, these waves are trapped just below the tropopause. Because the energy in trapped lee waves is not dissipated upward, air parcels may oscillate for many wavelengths downstream of the obstruction before being damped out. Such waves do not propagate upstream or vertically upward.

An indication of which of these two situations may exist can be found by calculating the Scorer parameter, l^2. This parameter is defined as:

$$l^2 = \frac{N^2}{U^2} - \frac{1}{U}\frac{d^2U}{dz^2} \tag{1.4}$$

where U is the wind velocity perpendicular to the mountain ridge. If the Scorer parameter decreases with height, then a trapping layer may exist, allowing for the formation of trapped lee waves (Scorer 1949).

Although the Scorer parameter gives a general, theoretical idea of when certain waves will form, the conditions for forming lee waves are highly dependent on the

specific topography at each location. Moreover, the equations which determine wave behavior are non-linear for large values of h/λ, where h is the height of the topography and λ is the wavelength of the lee wave (Durran 2003). As a result, both trapped and vertically-propagating lee waves may in fact exist at the same time. Waves which are "hybrid" between the two types may also exist (Glickman 2000).

Lee waves over the steep topography in the Sierra Nevada Mountains are particularly well-known. As Scorer observed, large-amplitude lee waves are more likely to form in response to steep features (Scorer 1949). On the eastern edge of the Sierra, the topography drops from 4,000 meters to 1,000 meters in a horizontal distance of about 10 kilometers. This slope connecting the Sierra Nevada with the Owens Valley is one of the steepest topographic gradients in the United States (Doyle et al. 2011). Accordingly, lee waves over the Owens Valley can be very strong.

The earliest data on Sierra Nevada lee waves come from the Sierra Wave Project, a measurement campaign conducted using sailplanes in the 1950s (Holmboe and Klieforth 1957). Their measurements observed large lee waves in the Sierra Nevada with wavelengths of 13-32 kilometers and associated vertical wind speeds of ± 9 m/s to ± 18 m/s. Smaller and less-severe waves were also observed during the Sierra Wave Project (Grubišić 2004).

Lee waves in the Sierra Nevada were studied again in 2006, with more sophisticated equipment, as part of a study called the Terrain-Induced Rotor Experiment (T-REX). Ground observations, balloon measurements, and flight data were collected on 22 days in March and April of 2006. This study was consistent with the 1950s study and provided more precise observations about the vertical and horizontal structure of the lee waves (Parish and Oolman 2012).

Importantly, the analysis of the T-REX experiments showed that strong lee waves in the Sierra Nevada occur when the prevailing winds are directed across the ridgeline and when the atmosphere near the peaks of the mountains is stable. Under these conditions, trapped lee waves are likely to form (Sheridan and Vosper 2012).

Chapter 2

Methods

For this project, several different types of data were used. In the following sections, the geodetic, geographic, and meteorological data used for this project are described. The analysis performed on the data is also described.

2.1 Sources of Data

- Plate Boundary Observatory (PBO) GPS dataset, including once-per-day output for 1,100 stations in the contiguous United States (http://pbo.unavco.org/data/gps)
- GPS data at 30-second resolution for selected stations and time intervals (RINEX files courtesy of PBO, http://pbo.unavco.org/data/gps)
- 90m-resolution topography data from the Shuttle Radar Topography Mission (http://www2.jpl.nasa.gov/srtm/)
- Numerical weather model output (North American Mesoscale model, http://nomads.ncep.noaa.gov/)
- Radiosonde observations of atmospheric parameters from the National Weather Service (http://weather.uwyo.edu/upperair/sounding.html)

- Moderate Resolution Imaging Spectroradiometer (MODIS) visible and infrared imagery (http://ladsweb.nascom.nasa.gov/)

2.2 Determining Skewness

The first step of the analysis was to determine which stations showed highly-asymmetric noise characteristics. Position time series were downloaded from the PBO website for each GPS station in the United States. A median filter with a window of 75 days was applied to each position time series in order to generate a time series that captured only the long-term trends. The output of the median filter was subtracted from each raw time series in order to remove such trends, including seasonal variations and long-term plate motions. The remainder was a set of daily position residuals. The highest and lowest 2% of residuals for each station were discarded to ignore cases of bad data. Then, the skewness of each remaining set of residuals was calculated.

Skewness,γ, is a statistical measure of the asymmetry of a dataset. For a random variable X, *skewness* is defined as:

$$\gamma = \sum_{i=1}^{n} \frac{1}{n} \left[\left(\frac{X_i - \mu}{\sigma} \right)^3 \right] \tag{2.1}$$

where X_i represents each value of the random variable, μ is the mean of X, σ is the standard deviation of X, and n is the number of observations. For a perfect Gaussian distribution or any other symmetric distribution, the skewness is exactly zero. For an asymmetric distribution, the sign of the skewness describes the direction of the "tail" of the asymmetric distribution.

At most GPS stations, we would expect the noise characteristics to roughly fit a Gaussian model; in other words, we would expect that all sources of non-random error are accounted for in data processing. Skewness values near zero would be expected for the set of residuals in such a situation. Longer time series at "Gaussian" stations would be expected to have skewness values closer to zero, although even the longest GPS records, at two to three thousand observations, may show some skewness due to

having finite number of data points.

To determine the bounds on skewness from Gaussian noise models, a Monte Carlo simulation was performed. A computer simulation with a random number generator produced many copies of a control dataset of Gaussianly-distributed random noise. Each dataset consisted of several thousand observations (matching the lengths of typical time series in the GPS data). The skewness of each simulated dataset was computed. 1000 instances of this random dataset were analyzed, giving bounds on the skewness values that are likely to result from a process described by a Gaussian noise model.

Subsequently, skewness values were calculated and tabulated for each GPS station using the residuals of the time series in the North, East, and Up directions. The results for selected stations are presented in Chapter 3.

A small number of stations were excluded from the analysis. Stations were excluded if they had fewer than two years of observations or if they had severe errors due to snow. The snow-related errors can be identified by a loss of data in the winter. The loss of data results from snow cover above the GPS antenna and on the solar panels, causing loss of power to the receiver.

2.3 Determining Spatial Patterns of Skewness

For each station, a two-dimensional vector was constructed from the skewness values for the North and East components:

$$\mathbf{v}_\gamma = \gamma_E \hat{\mathbf{x}} + \gamma_N \hat{\mathbf{y}}. \tag{2.2}$$

The purpose of this vector is to show the tendency for asymmetric outliers at each station. The direction of the vector represents the direction in which outliers are most likely, and the magnitude represents the likelihood of outliers in that direction. This two-dimensional vector was plotted on a map of local topography for each station.

At each station, the gradient vector of the local topography was also found and plotted on a map. The gradient was calculated using SRTM topographic data with 90-

meter resolution. In general, topographic gradients must be calculated with respect to a certain length scale. For example, the gradient at the scale of several hundred meters may be influenced by small valleys, while the gradient at the scale of several kilometers is likely to be influenced only by the overall shape of mountain ranges.

For this investigation, the topographic gradient at multiple length scales was investigated. The length scales ranged from 250 meters to 10 kilometers. A circle with the radius in question was drawn around each site, and the direction of maximum elevation increase around the circle was identified and plotted on a map. Then, the angle between the gradient vector and the skewness vector at each station was studied in order to determine the relationship between the asymmetric GPS outliers and nearby topographic features.

2.4 Determining Temporal Patterns of Skewness

Two types of weather information were gathered for comparison with GPS time series. One type of data came from radiosonde observations courtesy of the National Weather Service. The National Weather Service deploys radiosondes every 12 hours from major airports in the United States. The soundings provide measurements of temperature, pressure, and relative humidity as a function of elevation. For this analysis, radiosonde observations were analyzed from: Oakland, California; Reno, Nevada; Las Vegas, Nevada; and Vandenberg Air Force Base, California.

The second type of data analyzed was the output of a Numerical Weather Model (NWM). The NWM used in this project was the North American Mesoscale (NAM), one of several large computer models which solve the equations of motion for the atmosphere and project them forward in time to predict weather phenomena. The NAM uses a grid spacing of 12 km. Every six hours, the NAM automatically produces models of the 3D temperature, pressure, and wind fields over the entire United States. The models are consistent with the most recent radiosonde and satellite data.

For this project, the model output was used in lieu of actual observations in order to infer the temperature, pressure, and wind over remote regions of the Sierra

Nevada. The output of the NAM was downloaded from the National Weather Service online server. The data were processed using the GrADs software package in order to convert from compressed binary files to standard text files that could be analyzed by MATLAB and other software.

Both the radiosonde data and the NAM output were compared day-by-day with GPS time series at a number of locations in the Sierra Nevada. Correlations between specific atmospheric parameters and large outliers in the GPS data are presented in Chapter 4.

Daily satellite imagery was also used to identify correlations between the behavior of the atmosphere and large GPS outliers. The data came from the Moderate Resolution Imaging Spectroradiometer (MODIS) instrument on NASA's Terra and Aqua satellites. Images of the Sierra Nevada were inspected for lee waves both on the days which produced GPS outliers in that region and on the days which produced normal GPS results.

2.5 Examining Phase Residuals

For several stations in the Sierra Nevadas, patterns of phase residuals were studied on days with outliers and on surrounding days with normal (non-outlier) measurements. The phase residuals are an indication of un-modeled sources of error in each measurement, and they can reveal from which parts of the sky the errors arise.

During normal operation, each GPS station records a measurement from each visible satellite at 30-second intervals. The measurements include the phase of the signal (from 0 to 2π), the elevation angle of the satellite (from a cutoff of 10 degrees near the horizon to 90 degrees when completely overhead), and the azimuth angle of the satellite. Tens of thousands of such observations are combined to generate each daily estimate of position in the North, East, and Up coordinates.

The phase residual of each measurement is the difference between the phase of the incoming signal and the expected phase of that signal if each parameter estimate were accurate. When errors occur, some of the error is absorbed into the parameter

estimates (such as the position estimates) and some of the error is expressed in the phase residual. On days when position errors occur, the phase residuals contain information about any further errors that are not absorbed in the position displacement or the other parameter estimates.

All phase residuals over a 24-hour period for a given station were collected and the average phase residuals for each small block of the sky were displayed on a sky map as a function of the azimuth and elevation angle of the measurements. The root mean square (RMS) values of all phase residuals for the days in question were also calculated. Chapter 4 presents the sky maps for several highly-skewed stations on key days when position errors occur.

Chapter 3

General Results: Skewness in the PBO Network

In this chapter, I explore the general results of the skewness calculation for the PBO network of GPS stations. The approximately 1,100 stations in the network are classified by their skewness values. Then, the geographic distribution of the highly-skewed stations is presented in Section 3.1. In Section 3.2, the relationship between skewness at highly-skewed stations and the local topography at those stations is explored.

3.1 General Characteristics of Skewness in the PBO Network

For each station, the skewness was calculated for the North, East, and Up directions. The calculation showed that some stations have positive skewness values and others have negative values, but that the network as a whole shows no overall directionality. The skewness values are usually between 0 and ± 1.5. For example, the skewness values for selected stations across the United States are presented in Table 3.1. The skewness values in the East and North are shown along with the magnitude of the vector created by combining the two skewness values.

The last line of Table 3.1 shows the skewness values for P642, a station with very

high skewness values. For this study, P642 is an important example of a station with high skewness, as P642 and neighboring stations serve as the focus of later parts of this project (see Chapter 4).

Table 3.1: Skewness Values at Selected GPS Stations

Station	**Location**	$\gamma_{\mathbf{E}}$	$\gamma_{\mathbf{N}}$	$\|\mathbf{v}_\gamma\|$
BLA1	Virginia	0.10	0.01	0.10
WMOK	Oklahoma	0.04	0.21	0.21
RUBY	Nevada	0.16	-0.28	0.32
P363	Oregon	-0.21	-0.34	0.40
P642	California	-0.67	-1.30	1.46

The summarized results of the network-wide analysis are shown in Table 3.2. Each station is categorized based on the magnitude of its skewness vector (derived from the East and North time series data). Table 3.2 shows that the majority of stations have low skewness values below 0.25, but that many highly skewed stations also exist in the network.

Table 3.2: Skewness in the PBO Network of GPS Stations

Magnitude of Skewness	**Number of Stations**
$0.00 < \gamma < 0.25$	609
$0.25 < \gamma < 0.50$	285
$0.50 < \gamma < 0.75$	73
$0.75 < \gamma < 1.00$	48
$\gamma > 1.00$	46
Total	1061

Note that stations with small skewness are common, while stations with large skewness are relatively uncommon.

The Monte Carlo simulation described in Section 2.2 showed that at the 95% confidence level, the skewness of a dataset of several thousand data points described by a Gaussian noise model is between 0 and 0.2. By comparison, the PBO network of GPS stations has many stations with skewness values higher than 0.2. The distribution of skewness values shows that the noise characteristics at several hundred stations are not well-described by simple Gaussian models.

In particular, focusing on the cases with the highest skewness, there are 46 stations

in the United States whose skewness values are greater than one. The noise characteristics at these stations are very poorly-described by a Gaussian model, meaning that a source of non-Gaussian error is affecting measurements at these stations. I focus on these stations with especially high skewness values during the rest of the analysis.

The geographic locations of all stations are shown in Figure 3-1. Based on the classifications in Table 3.2, the 609 stations with skewness between 0 and 0.25 are shown in dark blue. The next 285 stations with skewness between 0.25 and 0.50 are mapped in a lighter blue. Each successive category of skewness values has an associated color on the map. At the upper extreme, the 46 stations with the highest skewness values ($\gamma > 1$) are shown in red.

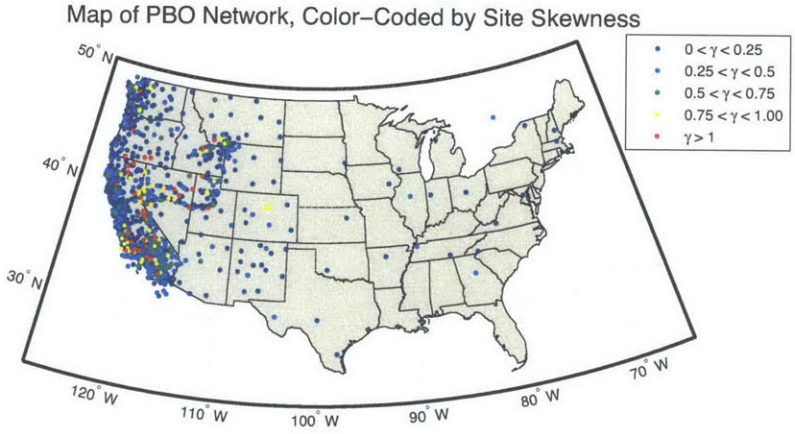

Figure 3-1: The PBO Network color-coded by station skewness. Red sites have the highest values of skewness.

It is observed that all stations with the highest level of skewness are located in the western half of the United States. This observation is not particularly surprising given the high density of stations in general in the Western US. Within this region, certain locations have a higher density of highly-skewed stations than others. The Sierra Nevada, the region north of Los Angeles, and the Basin and Range Province in Nevada and Utah have large numbers of skewed stations. Regions with particularly

low skewness values, besides the Eastern United States, include the Southwest and the Central Valley of California. The Central Valley, which can be seen more clearly in Figure 3-2, has almost no highly-skewed stations. Also, the dense network of stations in Yellowstone National Park shows almost no skewness at all.

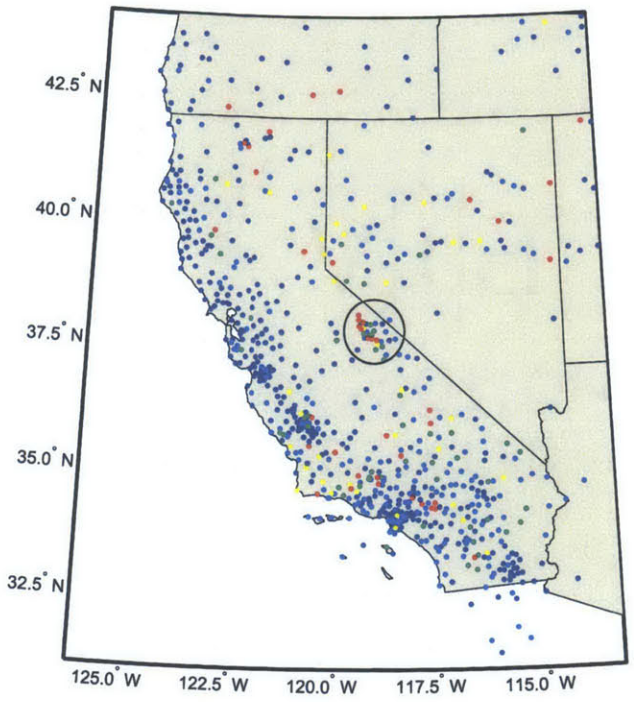

Figure 3-2: A map of the Western United States highlighting the dense region of highly-skewed stations in the eastern part of California. Another striking feature is the lack of skewed stations in the Central Valley.

One region deserves particular attention. On the eastern edge of the Sierra Nevada, highlighted in Figure 3-2, there is a region where highly-skewed stations are very common. Within the small, circled region near Mammoth Lakes, California, there are eight stations with high skewness. As this region contains a high density of skewed stations, it is an area of special interest for this project.

3.2 The Relationship Between Skewness and Local Topography

In this section, the vector created from the skewness values was plotted on a topographic map at each station. The direction of the skewness vector represents the direction in which outliers in the GPS data are most likely to occur. In many locations, it appears that the direction in which GPS outliers are most likely aligns with the direction to the nearest region of high topography.

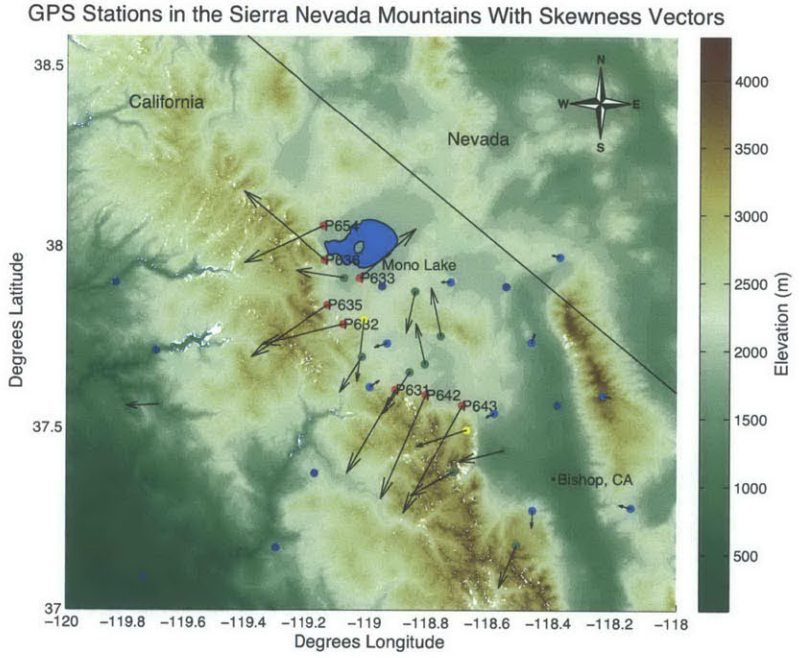

Figure 3-3: Skewness vectors on a topographic map of Mammoth Lakes, California. Arrows represent the direction and magnitude of the skewness vector.

For the Mammoth Lakes region, with its high density of skewed stations, it can be observed that many of the stations have skewness vectors that point uphill from the location of the station (Figure 3-3). For example, stations P631, P642, and P643, all located to the northwest of Bishop, CA, have skewness vectors pointed in the same direction. The skewness vectors seem to point towards the high mountains to the southwest of the stations.

The alignment between the local uphill direction and the skewness direction is also observed at many other highly-skewed stations in the network. Figure 3-4 highlights six GPS stations and shows the close alignment between the direction of skewness and the direction of the topographic gradient at each of them. Each station in this figure has $\gamma > 1$, putting it in the category of stations with the largest skewness. In Figure 3-4, the black circle surrounding each point was used to compute the topographic gradient.

The relationship between the direction of skewness and the topographic gradient vector was quantified by finding the angle θ between the two vectors. Small values of θ indicate a high degree of alignment between these two vectors.

Figure 3-5 shows the values of θ for all highly-skewed stations ($\gamma > 1$) with various topographic gradient vectors. The topographic gradient vector was calculated at length scales of 0.25 kilometers, 3 kilometers, 5 kilometers, and 10 kilometers.

For the smallest-scale topographic gradients, at the scale of hundreds of meters, the topographic gradient seems to be uncorrelated with the direction of the skewness vector (Histogram A in Figure 3-5). The histogram only shows a slight preference for small values of θ, which represent strong alignment between the two vectors. Similarly, topographic gradients at a scale of 10 kilometers (Histogram D) show weaker correlation with the direction of the skewness vector.

At length scales of 3 to 5 kilometers, however, there is often strong alignment between the skewness vectors and the topographic gradient vectors. In Histograms B and C, the majority of the θ values are small. This result suggests that topographic features at a scale of several kilometers can influence the direction of skewness at highly-skewed stations.

In summary, the problem of strongly skewed outliers suggests that an un-modeled source of error is affecting a specific group of GPS stations in the PBO network. Skewed outliers only appear to be a common phenomenon at 5-10% of the stations in the network. The tendency for skewed outliers is most common in mountainous regions like the Sierra Nevada and the Los Angeles area, and is less common in regions like the Eastern United States and the Central Valley of California. For highly-skewed

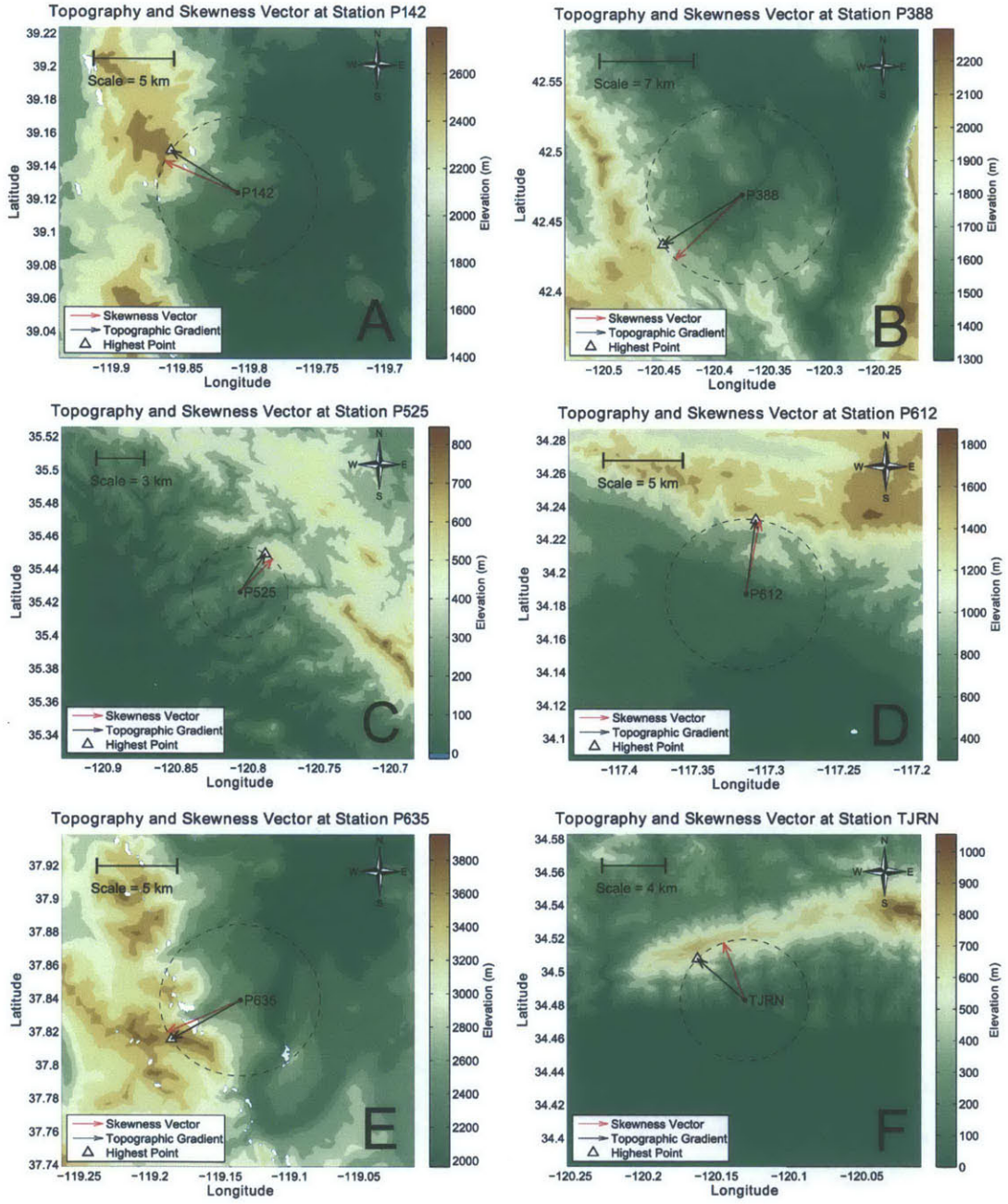

Figure 3-4: The alignment between skewness vector and locally high topography at six GPS stations: A) P142, Eastern Nevada; B) P388, Oregon; C) P525, Central California coast; D) P612, Los Angeles, California; E) P635, Mammoth Lakes, California; F) TJRN, Santa Barbara, California. Note that the angle between the skewness vector and the topographic gradient is small in each case.

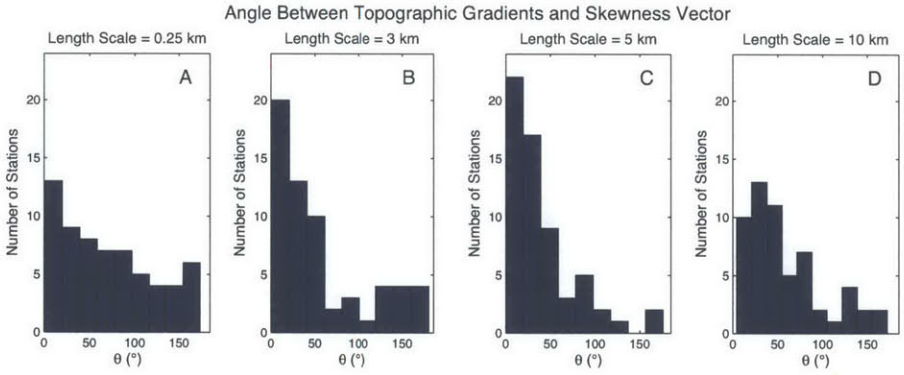

Figure 3-5: The relationship between topographic gradients and the skewness vector at various length scales. The histograms show distributions in the angle θ, the angle between the skewness vector and the local topographic gradient vector. The gradients at a scale of 3 to 5 kilometers are most closely aligned with the skewness vectors.

stations, the apparent alignment of the direction of the most likely GPS errors with the topographic gradient suggests that the source of the problem is somehow related to local topography at a length scale of several kilometers.

Chapter 4

Case Study: Outliers in the Sierra Nevada

In this chapter, I further explore asymmetric outliers at specific stations in the Sierra Nevada and on specific days. I focus on the weather conditions that existed in the Sierra Nevada on the days with outliers.

For this case study, I focus on stations P642 and P643, two stations near Mammoth Lakes, CA. These two stations both show large skewness values and are located only about 12 kilometers apart. In each case, the preferred orientation of erroneous GPS measurements is in a direction southwest of the actual station location. The Sierra Nevada Mountains are to the southwest of the stations.

P642 and P643 both show high skewness values and are both located in the Mammoth Lakes region, which is of interest for this project. As such, they served as prime examples for examining the effects of weather conditions on the skewness of GPS position outliers.

I focus on the relationship between position outliers and weather conditions for Sections 4.1-4.2. In Section 4.3, I examine the patterns of phase residuals across the sky at these two stations on several days with particularly large outliers.

4.1 NWM Results

The North American Mesoscale (NAM) Numerical Weather Model (NWM) produced wind velocity fields at given levels in the atmosphere for each day of the year. As an example, the wind field on November 30, 2012 at the 300 millibar surface is shown in Figure 4-1. The wind at the 300 millibar surface above the Sierra Nevada Mountains was blowing from the southwest with an average velocity of 21 meters/second. The 300 millibar surface, at approximately 9 kilometers elevation, was chosen for this analysis because the velocities at this level represent the large-scale flow of the atmosphere. At this elevation, velocities are uninfluenced by boundary-layer effects and are well above the peaks of the 4-kilometer-high Sierra Nevada Mountains.

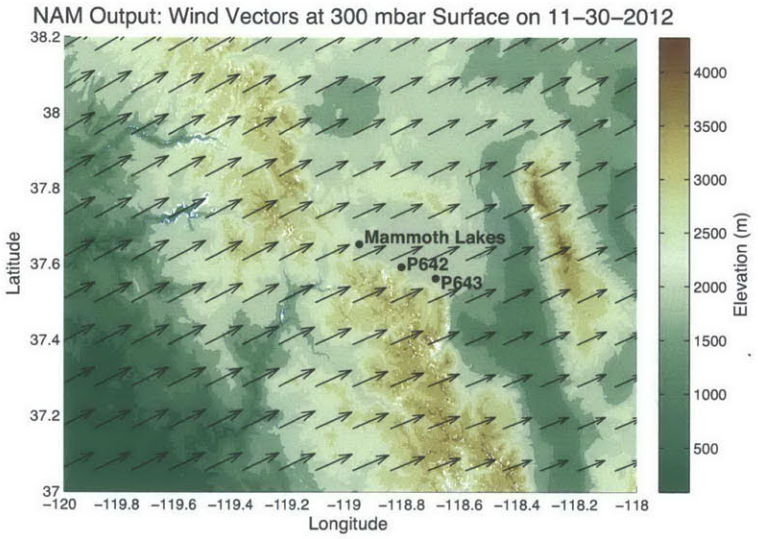

Figure 4-1: The NAM output on November 30, 2012 for the region above Mammoth Lakes, CA. The wind vectors shown are at the 300 millibar surface, which is at approximately 9 kilometers above sea level. The average velocity is 21 m/s.

Using the NAM output, the general patterns of wind velocity near Mammoth Lakes, California were found. For each day in 2012, the NAM output at the 300 millibar surface was collected and tabulated at the grid point closest to station P643 (Figure 4-2). The dataset is displayed in the form of a wind rose, a modified histogram that displays the probabilities of winds both at a given speed and in a given direction.

Plot A in Figure 4-2 shows the distribution of winds on days when the GPS data

at station P643 is normal, while Plot B shows the distribution of winds on the days with outliers that are the in largest 4% of all position deviations.

On days with typical (non-outlier) GPS measurements at station P643, the wind essentially always has a directional component blowing from west to east, which is consistent with the large-scale synoptic flow of the atmosphere over North America. Within that approximately 180 degree half-space, the range of possible wind directions is widely distributed. There is also high variability in the possible wind speeds.

However, on days with GPS outliers at station P643, the possible wind directions are restricted to a much narrower range. The winds blow from the west or the southwest on the days when outliers occur, and almost all of the outliers occur within a narrow range of about 30 degrees of direction. It can also be observed that winds on outlier days tend to have a higher magnitude than winds on non-outlier days. For example, in this dataset, there were no occurrences of outlier points on days having wind speeds below 20 m/s. An analogous plot made for station P642 shows similar results.

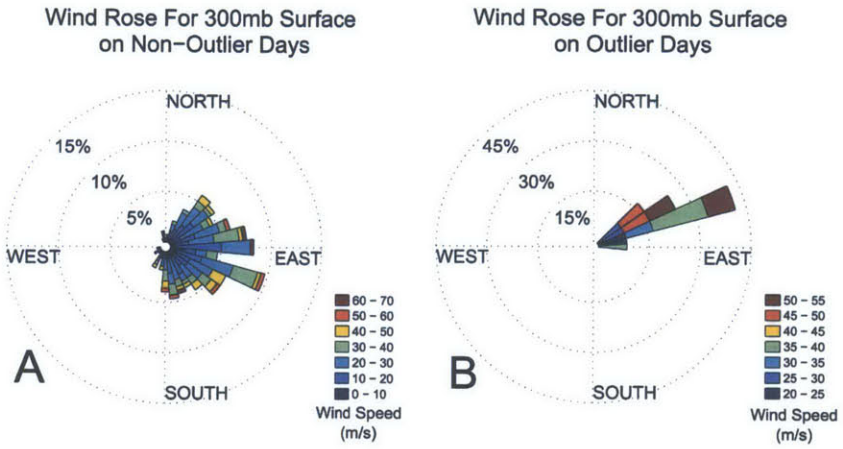

Figure 4-2: Wind roses for the NAM-derived wind velocity estimates at 300 millibar surface above station P643. Plot A shows the wind velocities on days with non-outliers in the GPS data at station P643, and Plot B shows the wind velocities on days with outliers in the GPS data at station P643.

The direction of the upper-level winds on days with GPS outliers at these two stations is notable because it is roughly perpendicular to the ridgeline of the Sierra

Nevada Mountains. This result will be discussed further in Chapter 5.

4.2 Radiosonde Results

Radiosonde measurements provide more dense coverage in the vertical direction than NWM's, so the radiosonde observations were used to study the vertical structure of the atmosphere on days with and without errors in the GPS measurements. The radiosondes were deployed twice per day at Oakland Airport, which is located 300 kilometers east (upstream) of the stations in question. The atmospheric parameters measured by the radiosondes, especially those at higher elevations, are not likely to change very much over this length scale.

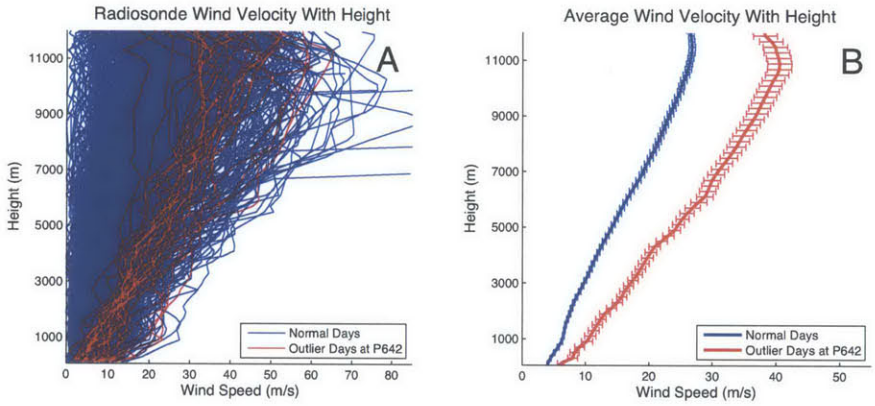

Figure 4-3: Plot A: Radiosonde-derived wind velocity as a function of elevation at Oakland during 2012. The GPS data are from station P642; red indicates that station P642 recorded an erroneous measurement within the highest 4% of its data on that day. Plot B: average wind velocity on outlier days and non-outlier days over the year. The error bars are the standard error of the mean velocity.

The primary observation from radiosonde data is that the days with outlier GPS measurements at certain stations have high wind speeds compared to the days with normal GPS position measurements (Figure 4-3). This result agrees very well with the results indicated by the NAM weather model. Furthermore, the radiosondes are able to show that this trend applies to the entire vertical profile of the wind speed above Oakland on outlier and non-outlier days.

In Figure 4-3, Plot A shows the velocity profile from each radiosonde measurement over the year. Plot B is derived from the same data and shows the average velocities on outlier days (red) and non-outlier days (blue). The error bars in Plot B are the standard deviation of each dataset divided by the square root of the number of data points in that dataset. Thus, the error bars on the figure represent the standard error of the mean velocity on days with and without GPS outliers. The error bars on the non-outlier days are smaller than the error bars on outlier days because there are many more non-outlier days in the dataset.

The amount of detail available in the vertical direction from the radiosonde data allows the Brunt-Väisälä frequency to be calculated for each day and compared between outlier days and non-outlier days (Figure 4-4). As in Figure 4-3, the error bars represent the standard error of the mean Brunt-Väisälä frequency on days with and without GPS outliers. The GPS station is station P642.

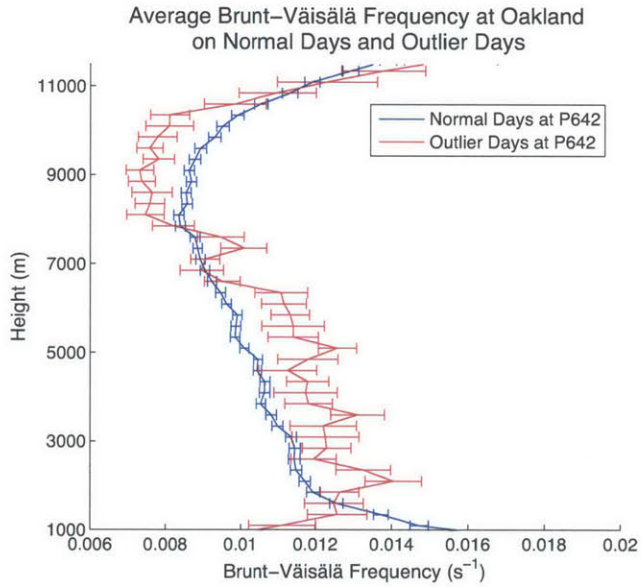

Figure 4-4: The average Brunt-Väisälä frequency as measured from Oakland Airport during the year 2012. The red curve represents the average Brunt-Väisälä frequency on days when station P642 recorded erroneous measurements within the highest 4% of its data.

It is notable that on outlier days, the average Brunt-Väisälä frequency is higher than normal between 3 and 7 kilometers elevation. On the same days, it is lower than

normal above 8 kilometers elevation. Since the Brunt-Väisälä frequency is related to the stability of the atmosphere, this result shows that the atmosphere has higher-than-average stability between 3 and 7 kilometers elevation on days with GPS outliers. The atmosphere also shows lower-than-average stability above 8 kilometers elevation on days with GPS outliers. This result will be discussed further in the context of lee waves in Chapter 5.

4.3 MODIS Results

A survey of MODIS images over California shows that lee waves to the east of the Sierra Nevada can be visually observed in satellite imagery on many of the days in which GPS outliers occur. In the images, the lee waves appear as closely-spaced rows of clouds parallel to the mountain range. The linear cloud formations show between two and ten wavelengths of lee waves.

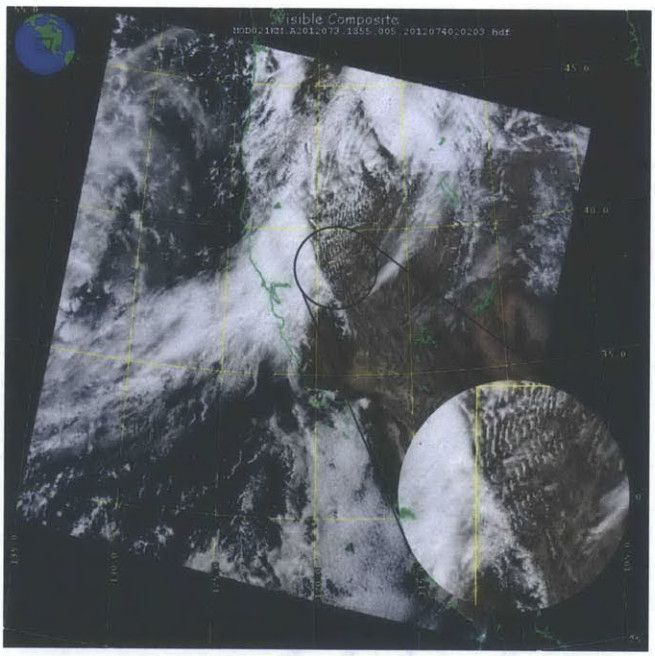

Figure 4-5: Lee waves in the Sierra Nevada on March 13, 2012, as observed by the MODIS instrument on NASA's Terra satellite.

For example, lee waves occurred over the Sierra Nevada on March 13, 2012, a

day when station P642 recorded a large outlier of 10.69 millimeters in the south-west direction (Figure 4-5). Interestingly, P643 recorded a displacement of only 1.28 millimeters on the same day. In the MODIS image, more than ten wavelengths of lee waves are visible downstream of Mammoth Lakes, CA. Based on this image, the wavelength of the lee waves was measured to be about 15 kilometers.

The occurrence rate of lee waves, as determined by a year-long survey of the MODIS image archive, is shown in Table 4.1. In general, lee waves appear in the MODIS images approximately one out of six days of the year.

However, the occurrence rate of lee waves in the MODIS images is much higher on days when stations P642 and P643 record outliers in the GPS data. On these days, lee waves are observed approximately two-thirds of the time.

Table 4.1: Lee Wave Observations from MODIS Satellite Imagery

Data set	**Total number of days**	**Lee wave days**
All days in 2012	366	63
Outlier days at P642	18	12
Outlier days at P643	18	11

4.4 Phase Residual Results

The phase residuals for P642 and P643 were analyzed on March 27, 28, and 29, 2012. Stations P642 and P643 each recorded position outliers during this period, but the largest outliers occurred on different days at these two stations. In MODIS images, lee waves were observed above the Sierra Nevada on all three of these days.

In the following plots, the phase residuals, which were originally dimensionless differences in phase, are multiplied by the wavelength of GPS signals (19 centimeters) in order to be expressed in millimeters. The phase residuals are shown as sky maps from the perspective of the receiver, so the East and West directions are opposite what they would be in normal plan-view.

Tens of thousands of individual GPS measurements are recorded daily at every station, each with an associated phase residual. The following maps show the local

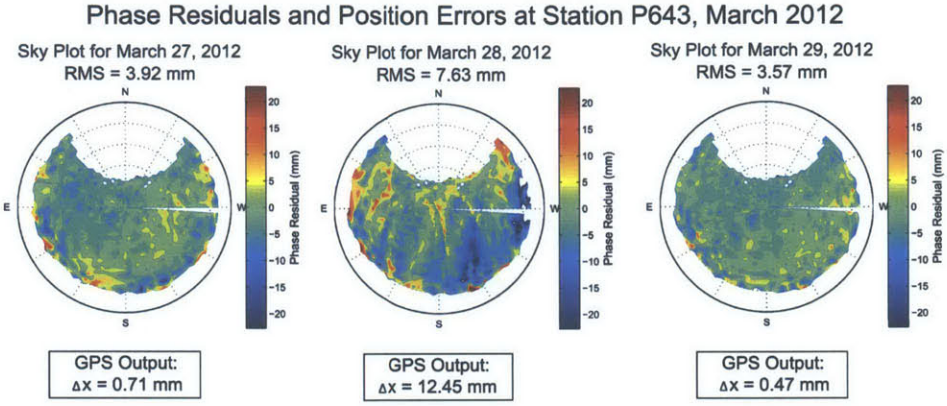

Figure 4-6: Sky maps of phase residuals at station P643. March 28, 2012 showed both elevated RMS scatter in the phase residuals and a large outlier in the GPS data. The surrounding days have lower phase residuals and normal position measurements.

averages of these phase residuals from different sections of the sky. Sky maps for P643 (Figure 4-6) and P642 ((Figure 4-7) are shown with the associated RMS values of the phase residuals for each day.

The systematic and non-random nature of the asymmetric outliers is clear when the phase residuals are compared with the position estimates. On the day with the largest outlier, March 28 at P643, the scatter of the phase residuals is elevated by about 100% when compared with normal days, but the position outlier is outside of the normal range of errors by a much larger margin.

It is also clear that elevated scatter in the phase residuals does not always correlate with position outliers. Some days with position outliers (e.g., March 27, 2012 at P642; Figure 4-7) show no unusual patterns of phase residuals but large position outliers.

The phase residuals show that the additional noise on days with position outliers is spatially correlated. It is not randomly-distributed across the sky. This observation suggests that weather patterns may be responsible for the elevated scatter in the phase residuals.

In summary, the meteorological portion of this project consisted of a comparison between GPS outliers and weather conditions, showing that upper-level winds are strong from the west-southwest direction on the days when outliers occur. The stability of the atmosphere follows certain trends with altitude on days when outliers

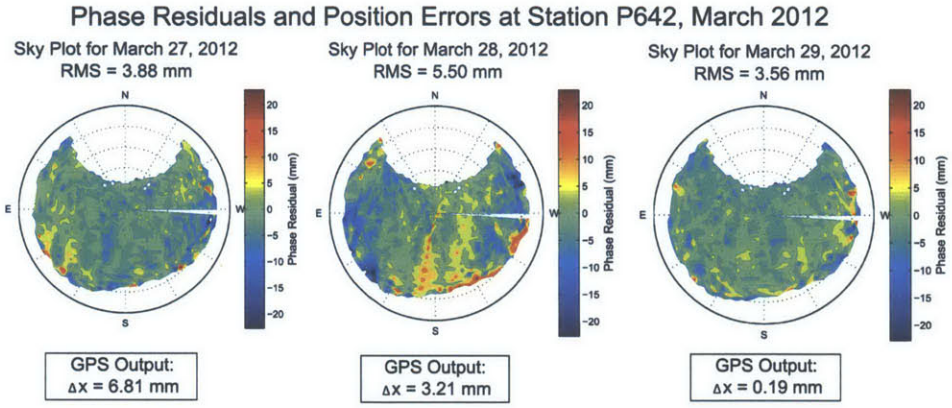

Figure 4-7: At station P642, a large outlier measurement (6.81 mm) was made on March 27, 2012. The phase residuals did not show higher scatter on that day. The phase residuals did show elevated RMS scatter on March 28, when the position measurement was in error by 3 millimeters.

occur. These patterns suggest that many of the conditions for the formation of lee waves are met on the days in question. Furthermore, satellite imagery confirms the presence of lee waves in the Sierra Nevada on many of the days when outliers occur at P642 and P643.

Scatter in phase residuals seems generally elevated on days with large GPS outliers, but not in every case. The elevated scatter suggests that the some of the error is being absorbed into parameter estimates (like the position estimates) and that some of the error is appearing in phase residuals. The sky maps of phase residuals show spatially correlated errors rather than random errors, consistent with the explanation that weather-related phenomena cause the outliers.

Chapter 5

Discussion and Conclusion

5.1 Summary and Interpretation of Results

The results presented in the previous chapters explain some of the general characteristics of skewness in the PBO network and the patterns of skewness at specific stations in the Sierra Nevada. Chapter 3 shows that the direction of skewed outliers at a GPS station is usually related to the uphill direction of the local topography at that station. For the specific cases of two GPS stations in the Sierra Nevada Mountains, Chapter 4 shows that GPS outliers occur only when certain atmospheric conditions are met.

In summary of these conditions, outliers occur when the winds at high levels of the atmosphere are strong and are blowing southwest-to-northeast, i.e. across the ridgeline of the Sierra Nevadas. The Brunt-Väisälä frequency shows that on days with GPS outliers, the stability of the atmosphere is higher than average at about the 4-kilometer level and lower than average at about the 9-kilometer level. A survey of MODIS images shows that on days when position outliers occur, parallel rows of clouds, indicative of lee waves, are more much likely to be seen in the satellite images than they are on a day chosen at random.

Although lee waves are very often seen in satellite images on outlier days, it is important to note that lee waves may occur on many more days than can be detected through satellite images. MODIS observations can only provide an incomplete

description of lee wave activity in the Sierra Nevada. The two satellites that carry MODIS instruments, both in sun-synchronous polar orbits, pass over a given location at around 10:30AM and 12:10PM local time. Any lee waves which develop in the afternoon or at night are not observable by these satellites. There are also conditions in which lee waves could occur without being observable from satellite images as the recognizable parallel rows of clouds. For example, lee waves are unlikely to be observed during extremely cloudy weather and extremely clear weather, as the relative humidity in the flow is not suitable for cloud formation and dissolution. Due to these factors, it is likely that lee waves in the Sierra Nevada occur on many more days than are presented in this report.

The patterns of atmospheric conditions on outlier days presented in Chapter 4, when interpreted in the context of lee wave formation, suggest that trapped lee waves rather than vertically-propagating lee waves are most likely occurring on the days in question. According to previous studies of lee wave dynamics, conditions with strong winds perpendicular to the ridge are favorable for the formation of lee waves in general (Sheridan and Vosper 2012). In particular, high atmospheric stability at the level of the mountaintops, as observed on the days with GPS outliers, is favorable for the formation of trapped lee waves (Sheridan and Vosper 2012). The highest peaks of the Sierra Nevada are at 4 kilometers elevation, and the stability of the atmosphere at this elevation is higher than normal on days with position outliers.

The Glossary of Meteorology provides a helpful definition of trapped lee waves which makes the connection even clearer. Trapped lee waves "occur within or beneath a layer of high static stability and moderate wind speeds at low levels of the troposphere (the lowest 1-5 km) lying beneath a layer of low stability and strong winds in the middle and upper troposphere" (Glickman 2000). This description matches almost exactly the conditions that occur when outliers are present. Thus, the calculation of the Brunt-Väisälä frequency in Chapter 4 (Figure 4-4) suggests that the lee waves coincident with the GPS position outliers are most likely trapped lee waves.

The trapping layer which stops the vertical propagation of these waves is the region of low stability at 8-9 kilometers altitude. The presence of this layer is inferred

from the low average Brunt-Väisälä frequency at this level on days with outliers.

The altitude of the trapping layer allows us to calculate the number of wavelengths of lee waves that are visible in the sky at a given GPS station. A typical GPS station in the Sierra Nevada is situated at about 2,000 meters elevation; the trapping layer at the top of the lee waves is then about 6 kilometers above the station. GPS receivers usually record signals above a cut-off angle of 10 degrees. For a 10 degree angle, the edge of visibility of the 6 kilometer surface is about 34 kilometers away in either direction. Therefore, for typical lee waves with wavelengths of 15 kilometers, a maximum of four wavelengths would be visible to a GPS station across the entire sky. Because lee waves are only formed on the downwind side of the mountain, it is more likely that only two or three wavelengths would be visible to a given GPS station. The oscillations would be concentrated in one side of the sky.

5.2 Possible Mechanisms for Position Errors

We can hypothesize several reasonable mechanisms for lee waves causing systematic positioning errors in GPS measurements. The first possible mechanism is based on the dry atmospheric delay alone; a second mechanism is based on the water vapor component of the atmospheric delay. A third possible mechanism is based on the combination of the first two mechanisms with the standard technique of gradient estimation.

The first possible mechanism is that the dry atmosphere causes unusual atmospheric delay patterns as a result of lee waves. One previous study has examined the effects of lee waves on the dry component of atmospheric delay for laser (rather than microwave) ranging systems (Hauser 1989). Hauser's paper found that by integrating the equations of motion for the atmosphere under lee wave conditions, non-hydrostatic corrections to the surface pressure could be obtained. These corrections are important for the laser ranging system because unlike current GPS analysis techniques, this system estimates atmospheric delay based on surface pressure measurements. Any dynamics in the atmosphere which change the surface pressure cause errors in the

delay estimates. For lee waves, the non-hydrostatic pressure corrections in Hauser's work were proportional to the vertical velocities in lee waves.

Hauser concluded that lee waves had a negligible impact on atmospheric delay (causing at maximum about 10 millimeters of position error at 20 degrees elevation angle). However, Hauser's paper investigated lee waves in the Davis mountain range in Texas, where lee wave phenomena and vertical velocities are weak compared to the Sierra Nevada. Hauser assumed wavelengths on the order of 100 kilometers for lee waves, which are much longer than the wavelengths of 15 kilometers observed in the MODIS images during this project. Additionally, the horizontal wind speeds were small in Hauser's study because the laser ranging system in question is closed due to bad weather when winds are higher than 20 meters/second.

Applying Hauser's calculations to the strong lee waves in the Sierra Nevada, I found that dry, non-hydrostatic pressure deviations from the passage of a lee wave could lead to up to 66 millimeters of additional delay on a path that is slanted at 20 degrees elevation angle. Although current GPS techniques do not calculate atmospheric delay estimates based on surface pressure measurements, this exercise still indicates that the dry component of the atmospheric delay could be especially complicated under lee wave conditions. I found that in the Sierra Nevadas, the delays due to non-hydrostatic pressure variations could potentially be much larger than Hauser suggested.

Delays due to water vapor may also contribute to the effects of lee waves on atmospheric delay. Hauser did not consider the effects of the water vapor component of atmospheric delay because his measurements used visible light, and for visible light systems the delays due to water vapor are 70 times smaller than they are for microwave systems (Hauser 1989). For GPS analysis, however, delays due to water vapor may be significant sources of error.

Shimada et al. (2002) have studied the effects of lee waves, and in particular the associated water vapor delays, on GPS positioning measurements during a 1997 lee wave event in Japan. Focusing on the wet component of atmospheric delay was reasonable in this setting because the lee waves were located in a coastal environment

where water vapor was probably abundant in the atmosphere. The lee waves during this event produced parallel rows of clouds that were observed from geostationary weather satellites. The waves created variations in the relative humidity of water vapor that were strong enough to induce repeated cycles of cloud formation and vaporization, potentially having an effect on the index of refraction of the atmosphere inside and outside of the clouds.

Using a high-resolution numerical weather model with a grid scale of 250 meters, Shimada et al. modeled the lee waves formed on the days in question. They calculated the water vapor delay in three dimensions and found that it varies periodically from place to place within the lee wave. They also found that the lee wave event caused systematic position errors for several nearby GPS stations. Interestingly, some stations experienced errors in the direction of the mountains which cause the lee waves (similar to the results in this project), but most stations appeared to experience position errors in the opposite direction. The direction of the position error appears related to where the station is located relative to the mountains which form the lee waves.

The Shimada paper found several examples of position deviations that are in the opposite direction from the position deviations found in the Sierra Nevada in the present work. Nevertheless, the Shimada paper supports the idea that significant position deviations (larger than 10 millimeters) can occur as a result of periodic variations in water vapor during lee wave events. The position errors occurred despite the estimation and application of gradients in the atmosphere during data processing.

The third possible mechanism for lee waves creating position displacements combines the results of the first two mechanisms with the GPS technique of estimating gradients in atmospheric delay. Assuming that either the dry component of atmospheric delay, the wet component of atmospheric delay, or both components vary periodically with position along the direction of propagation of the lee wave, it is possible that the current standard method, involving the estimation of linear gradients, leaves significant un-modeled asymmetry in the atmospheric delay pattern across the sky.

Because lee waves are large enough that only two or three wavelengths are visible in the sky at a given time, the concept of a single linear gradient may not be able to capture the associated patterns of atmospheric delay. This is especially likely also because lee waves only exist in one portion of the sky above the receiver.

5.3 Future Directions

There are many unanswered questions and potential future directions for this work. For example, one open question is why an outlier may occur at one station on a given day with lee waves, but a neighboring station may be relatively unaffected. This phenomenon was observed on March 13, 2012, when P642 recorded an outlier of 10.69 millimeters and P643 recorded a normal measurement of 1.28 millimeters. MODIS imagery observed many cycles of lee waves above both stations on that day (Figure 4-5). Similarly, another open question is why lee waves may occur on many days in the year and outliers only occur on some of those days.

Another future line of investigation is examining GPS outliers and possible lee wave events in other areas of the United States. Lee waves may also occur in other places where skewness in GPS outliers is observed. For example, the San Gabriel Mountains in Southern California contain several highly-skewed GPS sites, and are also known to create lee waves, although the lee waves are less famous than the lee waves of the Sierra Nevada. Lee wave events may or may not be able to explain skewed outliers at those sites.

The end goal of this project in the future would be to parameterize and solve for the causes of the asymmetric outliers in GPS analysis techniques. In the same way that estimating gradients was shown to improve the accuracy of GPS measurements in places with azimuthal asymmetry, estimating other parameters may be able to remove the effects of lee waves and other sources of asymmetry that are not well-explained by gradients.

If the erroneous position measurements at stations like P642 and P643 cannot be removed through more subtle parameter estimation, another future line of work

would be to examine the way error bars are determined for position measurements. Currently, the error bars on outlier days are not reflective of the true error expressed in the phase residuals and in the displaced position measurements on outlier days. These small error bars on outlier days suggest, unrealistically, that station positions may shift by several millimeters one day and then return to their normal positions the next day. Expanded error bars on the days with position displacements would be reflective of the fact that stations do not undergo actual displacement followed by a quick return to their normal positions.

In the future, if the effects of lee waves on positioning errors can be successfully estimated and parameterized, it is even possible that GPS data may become useful in detecting or imaging lee waves. Over the past few decades, GPS measurements have become increasingly useful tools for studying various atmospheric phenomena. GPS may eventually be able to resolve information about lee wave events from the associated patterns of atmospheric delay.

5.4 Conclusion

Asymmetric GPS position errors of 5-15 mm, often oriented in a preferred direction, have been seen to affect about 5-10% of the stations in the PBO network. In the interest of improving GPS accuracy for the affected stations in the PBO network, it is important to understand the distribution and cause of this phenomenon.

Topographic and weather data suggest that a coupling between the atmosphere and the topography is responsible for the asymmetric outlier patterns. Specifically in the Sierra Nevada, where asymmetric outliers are especially common, atmospheric lee waves are often observed on the same days as GPS position outliers. The conditions for trapped lee waves are almost always present when outliers occur at two example GPS stations near Mammoth Lakes, CA. Lee waves, which create unusual distributions of atmospheric delay in the sky, may be responsible for the errors in GPS position determination at these two example stations.

Considering the dozens of stations in the PBO network that are affected by the

problem of skewed outliers, it is important to identify a cause behind the problem. The observations in this project imply that positioning errors due to lee waves may be more common than previously thought. Future work into the effects of lee waves on GPS position estimates may help determine a solution to this problem.

The results of this project are especially applicable to campaign-style GPS measurements. Scientists conducting GPS campaigns in mountainous regions should be aware that without more sophisticated error modeling techniques, the occurrence of lee waves during an observation period could increase the error margin on GPS measurements. To obtain the most accurate measurements, scientists conducting GPS campaigns may wish to conduct their measurements on days when the weather conditions suggest that lee waves are not likely to occur.

Bibliography

[1] C. C. Chao. A new method to predict wet zenith range corrections from surface measurements. *Tech. Rep. Calif. Inst. Technol. Jet. Propul. Lab., 32-1256*, XIV:33–41, 1973.

[2] G. Chen and T. A. Herring. Effects of atmospheric azimuthal asymmetry on the analysis of space geodetic data. *Journal of Geophysical Research: Solid Earth*, 102(B9):20489–20502, September 1997.

[3] James D. Doyle, Qingfang Jiang, and Ronald B. Smith. Three-dimensional characteristics of stratospheric mountain waves during T-REX. *Monthly Weather Review*, 139(1):3–23, January 2011.

[4] D. R. Durran. In J. Pyle Holton, J.R. and J.A. Curry, editors, *Encyclopedia of Atmospheric Sciences*, volume 3, pages 1161–1169. Academic Press, London, 2003.

[5] Todd S. Glickman. *Glossary of Meteorology.* Boston : American Meteorological Society, 2000.

[6] Vanda Grubišić and John M. Lewis. Sierra wave project revisited: 50 years later. *Bulletin of the American Meteorological Society*, 85:1127–1142, 2004.

[7] James P. Hauser. Effects of deviations from hydrostatic equilibrium on atmospheric corrections to satellite and lunar laser range measurements. *Journal of Geophysical Research: Solid Earth*, 94(B8):10182–10186, August 1989.

[8] Jorgen Holmboe and Harold Klieforth. Investigations of mountain lee waves and the air flow over the Sierra Nevada. Department of Meteorology, UCLA Final Rep. Contract AF 19(604)728, 283 pp., 1957.

[9] Thomas R. Parish and Larry D. Oolman. Isobaric height perturbations associated with mountain waves measured by aircraft during the terrain-induced rotor experiment. *Journal of Atmospheric & Oceanic Technology*, 29(12):1825–1834, December 2012.

[10] R. S. Scorer. Theory of waves in the lee of mountains. *Quarterly Journal of the Royal Meteorological Society*, 75(323):41–56, January 1949.

[11] Peter Sheridan and Simon Vosper. High-resolution simulations of lee waves and downslope winds over the Sierra Nevada during T-REX IOP 6. *Journal of Applied Meteorology & Climatology*, 51(7):1333–1352, July 2012.

[12] S. Shimada, H. Seko, H. Nakamura, K. Aonashi, and T.A. Herring. The impact of atmospheric mountain lee waves on systematic geodetic errors observed using the Global Positioning System. *Earth, Planets and Space*, 54(4):425–430, January 2002.

[13] Ernest Smith and Stanley Weintraub. The constants in the equation for atmospheric refractive index at radio frequencies. *Proceedings of the IRE*, 41:1035–1037, 1953.

[14] Ronald B. Smith, Bryan K. Woods, Jorgen Jensen, William A. Cooper, James D. Doyle, Qingfang Jiang, and Vanda Grubišić. Mountain waves entering the stratosphere. *Journal of the Atmospheric Sciences*, 65(8):2543–2562, August 2008.

[15] David M. Tralli, Timothy H. Dixon, and Scott A. Stephens. Effect of wet tropospheric path delays on estimation of geodetic baselines in the Gulf of California using the Global Positioning System. *Journal of Geophysical Research: Solid Earth*, 93(B6):6545–6557, June 1988.